



Metal flowing and microstructure characteristics of the micro inner gear ring fabricated by rheological extrusion

Hong Jiang¹ · Peng Dong² · Peng Zhang³ · Yongfei Wang^{1,4} · Long An⁵ · Hao Li⁶ · Shengdun Zhao¹

Received: 30 November 2023 / Accepted: 1 February 2024 / Published online: 10 February 2024
© The Author(s), under exclusive licence to Springer-Verlag London Ltd., part of Springer Nature 2024

Abstract

The 2A50 aluminum alloy micro inner gear rings were fabricated using a rheological extrusion process. Metal flowing and microstructure characteristics of the micro inner gear rings in rheological extrusion were investigated by finite element simulation and experiments, respectively. The microstructures of the tooth, bottom land, and non-dentiform region were considered as representative sections of the inner gear ring. Results reveal that during the rheological extrusion process, the metal exhibited a continuous flow from the periphery toward the center of the billet along the radial direction, meticulously filling the tooth spaces of the mandrel. Concurrently, a gradual decline in flow velocity was observed. The grains in the teeth and bottom lands were fine and elongated along the flowing lines, whereas those in the non-dentiform region were similar to the semi-solid slurry with nearly equiaxed grains. The microstructure of the micro inner gear rings predominantly consisted of recrystallized grains and substructures. In non-dentiform regions, the proportion of recrystallized grains was remarkably higher than that of the substructure. The average grain size of the microstructure of the inner gear ring ranged between 14.04 and 20.05 μm . The grain size in the tooth was sensitive to the extruded temperature and showed an increment of approximately 36.3% when the temperature increased from 575 °C to 590 °C. This phenomenon suggests that low temperature in the semi-solid range was advantageous for the microstructure and mechanical performance of the inner gear ring. No pronounced texture was detected in the micro inner gear rings, and the peak intensity (4.81) in the pole figures was found in the bottom land at the extruded temperature of 590 °C, suggesting a relatively weak $\{112\} \langle 126 \rangle$ texture. This process recommends a propitious technique for the fabrication of components with microfeatures.

Keywords Micro inner gear ring · Rheological extrusion · Microstructure · Recrystallization · Texture

1 Introduction

Metal micro inner gear rings are crucial elements in the micro gear transmission system, functioning through engagement with micro gears to initiate the rotation or translation of specific components. These metal micro inner gear rings are widely applied in some compact precision structures, such as cameras, medical devices, and micro-robotics [1–3]. Traditional fabrication methods for these micro gear parts include powder injection [2], wire-cut electrical discharge machining [4], and laser processing [5, 6]. However, these techniques often face challenges like internal porosity, inefficiency in production, high costs, and limitations on billet thickness. Consequently, plastic forming methods have gained prominence due to their superior mechanical properties and good economy. Yang et al. [7] proposed a warm mold continuous casting process to create QAl9–4 aluminum bronze spur gear with excellent surface quality. They further investigated the influence of α grains and

✉ Shengdun Zhao
sdzhao@mail.xjtu.edu.cn

¹ School of Mechanical Engineering, Xi'an Jiaotong University, Xi'an 710049, China

² College of Mechanical & Electrical Engineering, Shaanxi University of Science & Technology, Xi'an 710021, China

³ College of Mechanical Engineering, Xi'an University of Science and Technology, Xi'an 710054, China

⁴ National Key Laboratory of Metal Forming Technology and Heavy Equipment, Xi'an 710049, China

⁵ AVIC Xi'an Flight Automatic Control Research Institute, Xi'an 710076, China

⁶ Shanghai BYD Company Limited, Shanghai 201605, China

precipitates on the mechanical properties of the gear. Yan et al. [8] employed hot extrusion to produce Ti-6Al-4V titanium alloy micro gears, focusing on the impact of holding time on both the extrusion force and the billet's microstructure before extrusion. Hu et al. [9] innovated a micro blanking device for fabricating H62 brass alloy micro internal gears and simulated the blanking process of internal gears with DEFORM. Unfortunately, these studies did not delve into the microstructure characteristics of the formed gears. Rohrmoser et al. [10] introduced a multipass cold forming process that combines extrusion and shear cutting for copper alloy miniature gears, but the dies suffered from high forming force. Jiang et al. [11] manufactured copper alloy miniature cup-shaped internal gears through a cold extrusion process and analyzed the influence of annealing temperature on the grain size. They discovered that the cold extrusion minimally influences grain refinement, with large initial grains leading to poor filling of the tooth profile.

Micro inner gear rings are cylinder components characterized by intricate microfeatures on their inner wall. These microfeatures significantly influence the forming process and mechanical properties of the components, thereby determining their application range and service life. Shear deformation can be enhanced in these microfeatures during the forming process through the strategic design of dies, subsequently leading to reliable forming quality and superior mechanical properties in the final product. Yan et al. [12] proposed a novel extrusion process involving slots at the punch bottom to generate microfeatures that increase shear deformation, thus improving the material flow from the punch bottom toward the cylinder wall. They analyzed the influence of shear grooves on the microstructure of the ZK60 cylinder part and discovered that dynamic recrystallization was the primary grain refinement mechanism, resulting in improved mechanical properties. Similarly, Che et al. [13] observed that additional grooves facilitated the metal flow from the punch bottom to the tubular wall, refining grains, weakening the strength of the texture produced during the extrusion process, and increasing the micro-hardness of the AZ80 tubular parts. Zhang et al. [14] explored metal filling in the tooth during the rolling process of thread shafts. They found that the grains at the outer edge of the tooth were elongated and refined, and the grain size at the top of the tooth was slightly larger compared to the bottom. Zeng et al. [15] prepared Ti-6Al-4V micro gears through the electrically assisted extrusion process and analyzed the effect of holding time on forming quality and microstructure. They observed severe plastic deformation and grain refinement at the gear tips. Gao et al. [16] conducted numerical and experimental investigations on the roll-forming process to produce micro-grooves on Cu plates,

observing fiber streamlines as metal flowed to the riblet peak. They concluded that multipass roll-forming was superior to a single-pass approach in shaping micro-grooves. Liu et al. [17] reported that low extrusion speed yielded excellent geometry and surface quality in the micro-grooves of the miniature heat pipe during the micro-extrusion process, although ultra-large extrusion ratios resulted in coarser grains in these regions, with high extrusion speed inhibiting grain refinement. Wang et al. [18] executed the micro punch process to fabricating Cu/Ni clad foils and recognized that refined grains at lower annealing temperatures caused less thinning of the Cu foil in the micro-channel. Conversely, coarse grains at higher annealing temperatures led to necking and surface waviness of the foil, which was detrimental to the microchannel. Su et al. [19] analyzed the filling quality, surface quality, and microstructure evolution of the micro ribs during the micro-embossing process of pure aluminum with coarse and ultrafine grains.

In summary, exploring the deformation mechanism and detailed microstructure of these microfeatures has a guiding significance for the reasonable choice of processing parameters and the improvement of the mechanical performance of the products. These components with microfeatures are similar to micro inner gear rings. The rheological extrusion emerges as a novel approach for the production of such micro-scale components. However, the literatures on rheological extrusion pertaining to micro components with microfeatures are relatively scarce. In this study, an innovative rheological extrusion forming process integrating shear deformation was introduced for fabricating 2A50 aluminum alloy micro inner gear rings. The metal flow behavior throughout the extrusion process was analyzed by finite element (FE) simulation. A comprehensive microstructural analysis of the tooth, bottom land, and non-dentiform region of the inner gear rings was conducted. Moreover, the impact of temperature on the microstructure of these regions was explored. The goal of this work is to offer a fresh perspective on the forming processes applicable to components with fine microfeatures, potentially refining the manufacturing techniques in industries requiring high precision, such as aerospace and biomedical engineering.

2 Numerical simulation and experiment methods

2.1 Materials properties

A 2A50 aluminum alloy was used in this work; its basic compositions and physical properties are shown in Table 1

Table 1 Chemical composition of the 2A50 aluminum alloy in wt%

Element	Si	Fe	Cu	Mn	Mg	Ni	Zn	Ti	Al
wt%	1.15	0.23	2.14	0.59	0.73	0.02	0.02	0.10	Bal

Table 2 Basic parameters of the 2A50 aluminum alloy

Young's modulus (GPa)	Poisson' ratio	Density (g·cm ⁻³)	Coefficient of thermal expansion (K ⁻¹)	Thermal conductivity (W·m ⁻¹ ·K ⁻¹)	Heat capacity (J·g ⁻¹ ·k ⁻¹)	Emissivity coefficient
70	0.3	2.81	22×10 ⁻⁶	185	8.75	0.7

Fig. 1 (a) Main dimensions of the micro inner gear ring; (b) FE model of the rheological extrusion

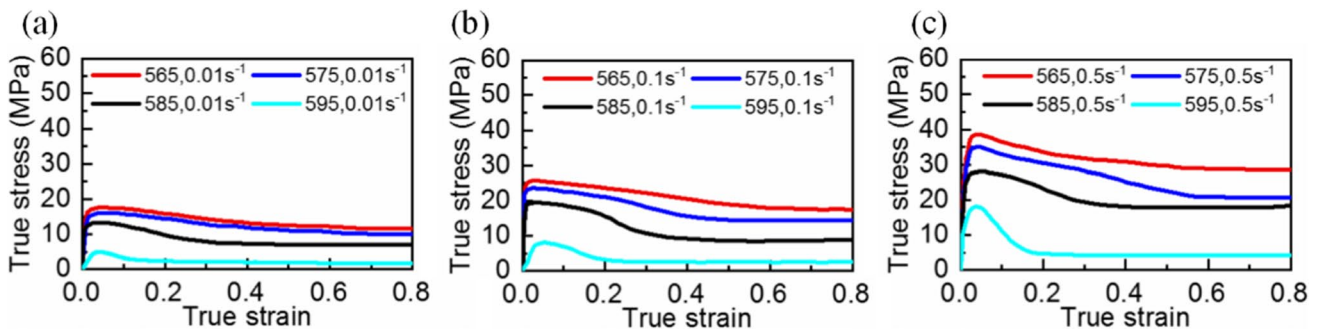
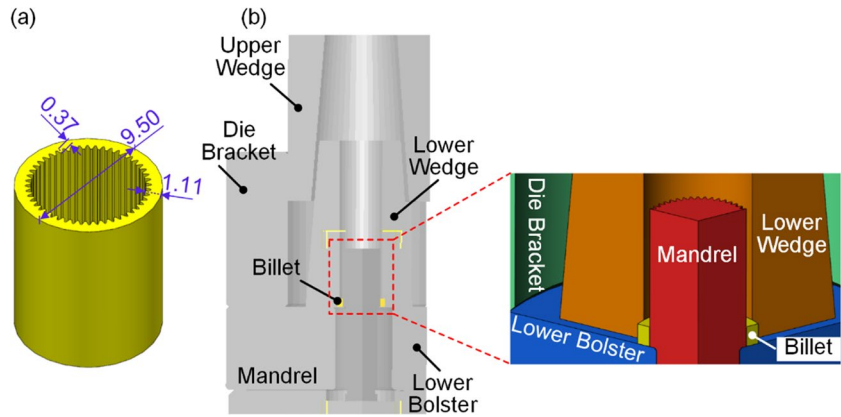


Fig. 2 True stress–strain curves of the 2A50 aluminum alloy under different strain rates: (a) 0.01 s⁻¹, (b) 0.1 s⁻¹, and (c) 0.5 s⁻¹

and 2, respectively. According to the previous work [20], the solidus and liquidus temperatures of the 2A50 aluminum alloy tested by DSC curves are 525.8 °C and 612.9 °C, respectively.

2.2 Numerical simulation

DEFORM-3D software was applied to simulate the rheological extrusion process of the 2A50 aluminum alloy micro inner gear ring to explore the flowing and filling of the material. The main dimensions of the micro inner gear ring are displayed in Fig. 1a, with a module of 0.15, a teeth number of 48, an addendum height of 0.12 mm, a dedendum height of 0.25 mm, and an outer ring diameter of 9.5 mm. The FE model shown in Fig. 1b mainly consists of upper wedge, lower wedge, billet, mandrel, die bracket, and lower bolster. All dies were defined as rigid bodies except for the billet.

Table 3 Basic setting parameters of the FE model

Basic parameter	Value and unit
Billet temperature	575 °C
Dies temperature	575 °C
The speed of the three lower wedges	0.087 mm/s (other dies were fixed)
Friction coefficient [21, 22]	0.3
Heat transfer coefficient	5 N/(s·mm·°C)
Element number of the billet	145,166 (including a refined mesh window with a size of 0.035mm)

In the pre-processing of the FE simulation, the true stress–strain curves obtained from the previous work [20] were imported into DEFORM-3D as the material curves, as shown in Fig. 2. The main setting parameters in the FE

model are shown in Table 3. The movements of the dies were simplified to efficiently simulate the extrusion process, where the lower wedge was moved radially toward the center of the billet with a velocity of 0.087 mm/s, and other dies were fixed. The model with 1/8 height and 1/3 circumferential section was used for analysis (Fig. 1b) to save calculation time. The symmetry conditions were set at the circumferential cutting planes because the original billet was a hollow cylinder.

2.3 Experiment procedure

2.3.1 Rheological extrusion process

The rheological extrusion process employed to fabricate the 2A50 aluminum alloy micro inner gear ring is depicted in Fig. 3. The billets with an outer diameter of 10.4 mm, an inner diameter of 7.7 mm, and a height of 8.5 mm were cut from the radially forged bar. The radial forging process aims to achieve substantial plastic deformation before the billet is subjected to isothermal treatment, facilitating the preparation of semi-solid slurries characterized by nearly spherical grains. After heating the dies and the billet for a certain period of time, these nearly spherical grains will emerge in

the billet, which is then subjected to rheological extrusion under the action of the dies.

In this work, the rheological extrusion experiments were performed on an Instron-5982 material testing machine with a die assembly illustrated in Fig. 4, where the induction heating coil is a supplementary accessory. The dies were assembled with screws, and then the billet, upper and lower wedges were placed into the assembly, as demonstrated in Fig. 3. The compression plate of Instron-5982 was securely in contact with the upper wedge before extrusion. The dies and billet were heated by the induction heating coil. When the dies and the billet were held at 575 °C for 3 min, the billet was expected to achieve a semi-solid microstructure with near-spherical grains, followed by rheological extrusion with the upper wedge moving down at a velocity of 1 mm/s under the driving of compression plate. When the extrusion was completed, the dies were rapidly cooled down with a high-powered blower, and the inner gear ring was removed from the dies once cooling to 200 °C. To study the microstructure of the micro inner gear ring extruded at different extrusion temperatures (T), the dies and the billet were held at 590 °C for 3 min, and then, the rheological extrusion experiment was performed again in the same step. The rheological extrusion at each temperature was carried out three times to ensure the accuracy and repeatability of the experiment.

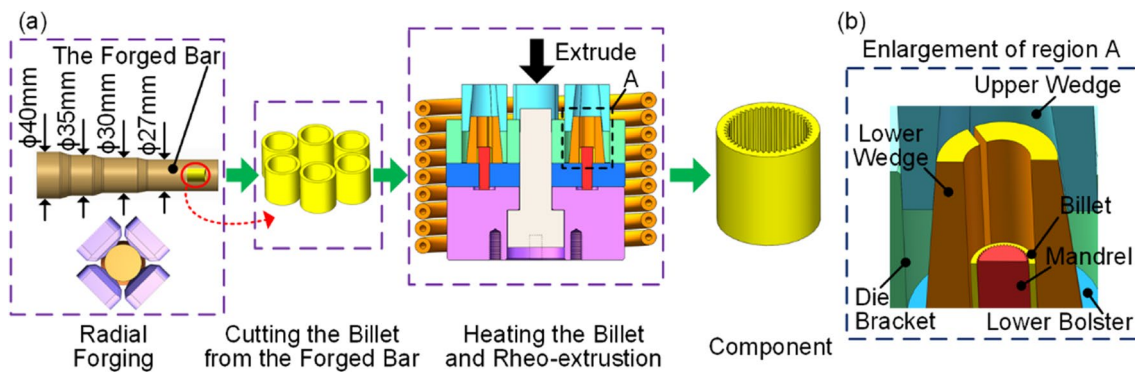
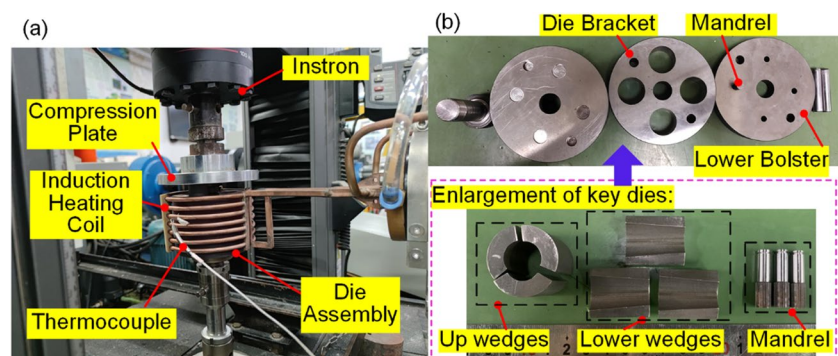


Fig. 3 (a) Scheme for the rheological extrusion process of the 2A50 aluminum alloy micro inner gear ring; (b) enlargement of region A

Fig. 4 Dies and equipment for the rheological extrusion experiment: (a) die assembly and Instron-5982; (b) main parts of the die assembly



The wedge faces of the upper and lower wedges are tangent to each other once all dies are assembled. The lower wedge is induced by these tangent wedge surfaces when the upper wedge is pushed down by the compression plate of the Instron-5982, thus moving horizontally and radially to the billet. This horizontal motion enables the lower wedge to move radially along the cylindrical billet, causing the metal to fill into a mandrel in the whole circumference of the billet. The velocity relationship between the upper and lower wedges is illustrated in Fig. 5.

The velocity relationship between the upper and lower wedge shown in Fig. 5 can be described as follows:

$$V_{2x} = V \sin \theta \cos \theta \quad (1)$$

where v_{2x} is the horizontal velocity of the lower wedge (mm/s), θ is the wedge angle of the wedge surface ($^\circ$), and v is the vertical downward velocity of the upper wedge (mm/s). The dimensions of wedges used in the simulation and experiment are identical, and θ is 5° . The vertical velocity (v) of the upper wedge is 1 mm/s in the extrusion experiment. According to Eq. (1), the horizontal velocity (v_{2x}) of the lower wedge is calculated as 0.087 mm/s, which aligns with the velocity of the lower wedge in the FE simulation (Table 3).

Samples were cut from the radially forged 2A50 aluminum alloy bar for isothermal treatment, that is, held at 575 $^\circ\text{C}$ and 590 $^\circ\text{C}$ for 3 min and then quenched into the water to preserve the semi-solid microstructure. This process aims to compare the microstructure of the extruded gears with that of the semi-solid billets obtained by isothermal treatment.

2.3.2 Microstructure characterization

All samples were embedded with resin powder. Sandpapers with the grit sizes of 200 #, 600 #, 800 #, 1000 #, and 2000 #

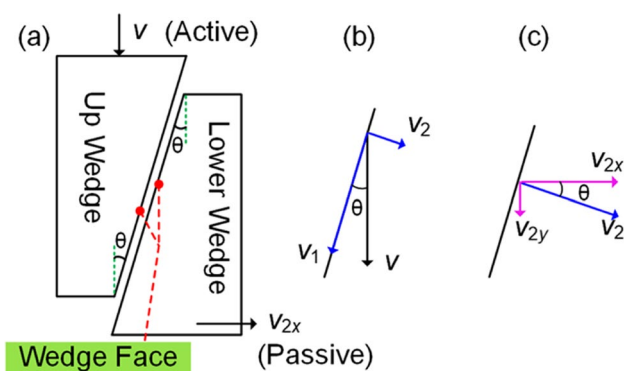


Fig. 5 Relationship of the velocity of the upper wedge and lower wedge: (a) position of the two wedges, (c) the components of the upper wedge velocity along and perpendicular to the wedge face, and (e) horizontal and vertical components of the lower wedge velocity

were used to polish the above samples from isothermal treatment and extruded micro inner gear rings. Subsequently, all samples were polished using diamond polishing agents with particle sizes of 2.5 μm , 1 μm , and 0.5 μm . The isothermal treatment samples were etched for 40 s in a 5% HF solution and observed with an optical microscope. In addition, the samples from micro inner gear rings were further polished with an ion thinning instrument (Leica EM RES102) for detailed microstructure analysis by Electron Back Scatter Diffraction (EBSD). The EBSD analysis was conducted on a scanning electron microscope (SU3500) equipped with an EBSD detector with an acceleration voltage of 15 kV. The scanning step size of the bottom lands and non-dentiform regions was 0.5 μm , whereas that of the teeth was 0.7 μm . The Oxford HKL Channel 5 software was used for analysis.

3 Numerical and experimental results

3.1 Metal flow and strain distribution

Figure 6 demonstrates the metal flow and filling into the mandrel during the rheological extrusion process of a micro inner gear ring. According to the gear tooth nomenclature [23], the characteristic regions of the inner gear ring are labeled in Fig. 6, including the top land, bottom land, tooth, and tooth space. Figures 3b and 6 show that during the radial advancement of the lower wedge, the inner side of the billet gradually approached the tooth flanks of the mandrel, and the metal filled into the tooth spaces. According to Fig. 6, the metal mainly flowed radially from the outer side to the inner side of the billet. With the continuous advancement of the lower wedge (S denotes the displacement of the lower wedge), the metal flow velocity at the tooth decreased from 0.095 to 0.01 mm/s, whereas that at the non-dentiform region near the outer side of the billet diminished from 0.084 to 0.06 mm/s. The flow of the metal toward the tooth spaces was intensely hindered by the bottom lands of the mandrel, resulting in the formation of the top lands of the micro inner gear ring.

The strain distribution during the rheological extrusion of the 2A50 aluminum alloy inner gear ring is shown in Fig. 7. The overall strain of the billet rose with the continuous motion of the lower wedge. The strain is inhomogeneous in the different regions of the billet, with the magnitude arranged as bottom land > top land > non-dentiform region. The strain on the tooth is larger than that on the non-dentiform region.

3.2 Morphology of the extruded micro inner gear ring

The macroscopic morphology of the micro inner gear rings after rheological extrusion at 575 $^\circ\text{C}$ and 590 $^\circ\text{C}$ is shown in

Fig. 6 Metal flow and velocity during the rheological extrusion process

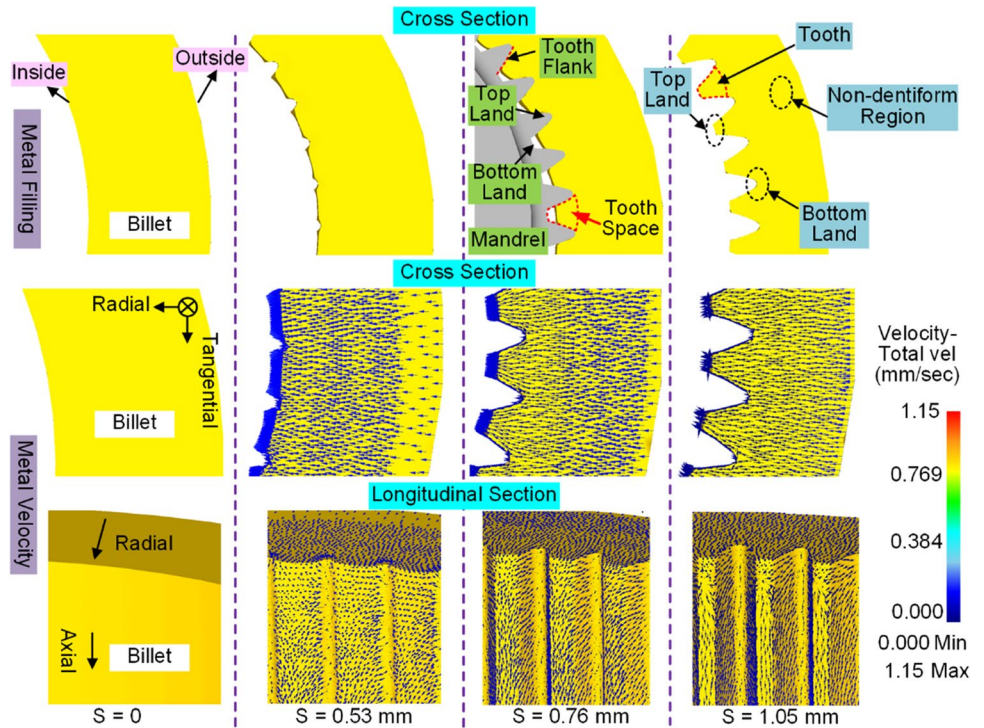


Fig. 7 Strain distribution during the rheological extrusion process

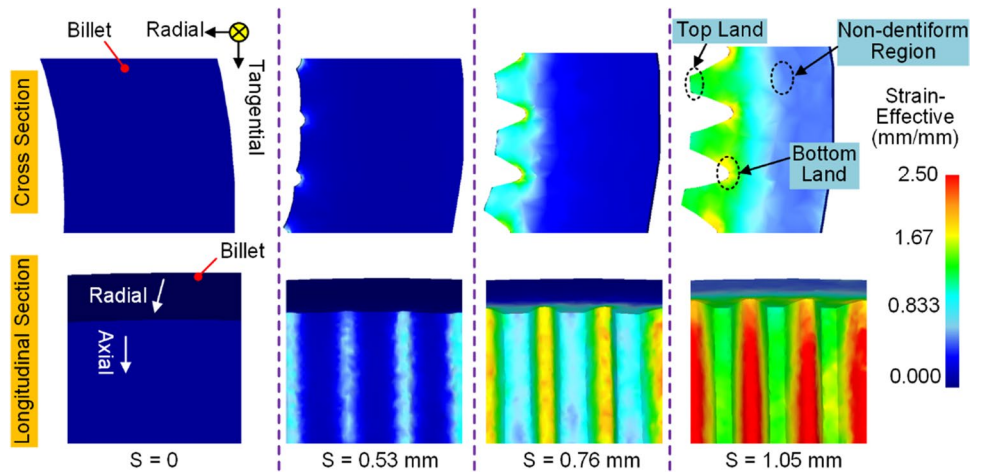


Fig. 8. The tooth profiles of the extruded inner gear rings are overall complete. The teeth and bottom lands are distributed continuously along the height direction without any apparent imperfections. The tooth profiles of the micro inner gear ring extruded at 575 °C were more regular and fuller and had fewer defects than those at 590 °C, as shown by the comparison between the cross sections of the inner gear rings (Fig. 8c, d).

3.3 Microstructure characterization

3.3.1 Grain size and grain boundaries

The microstructure of the 2A50 aluminum alloy radially forged bar after isothermal treatment is shown in Fig. 9. Typical semi-solid microstructure composed of homogeneous

Fig. 8 Macrographs of the micro inner gear rings under different extruded temperatures: (a) top view, $T=575\text{ }^{\circ}\text{C}$; (b) side view, $T=575\text{ }^{\circ}\text{C}$; (c) cross-section, $T=575\text{ }^{\circ}\text{C}$; (d) cross-section, $T=590\text{ }^{\circ}\text{C}$

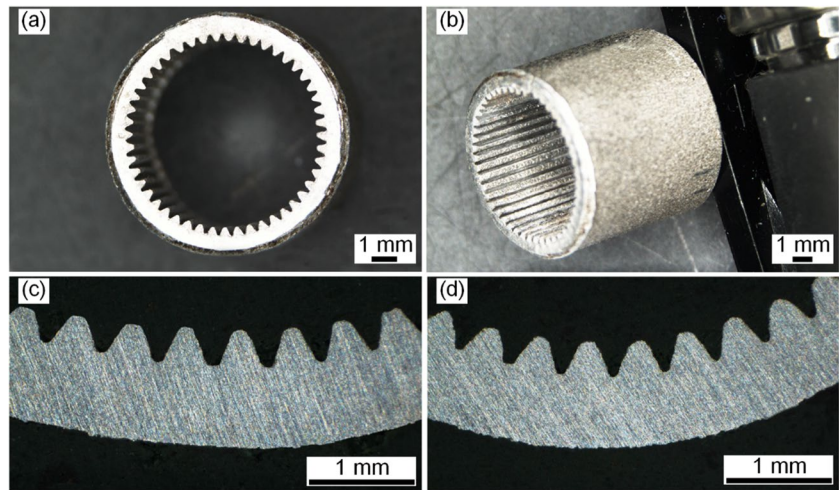
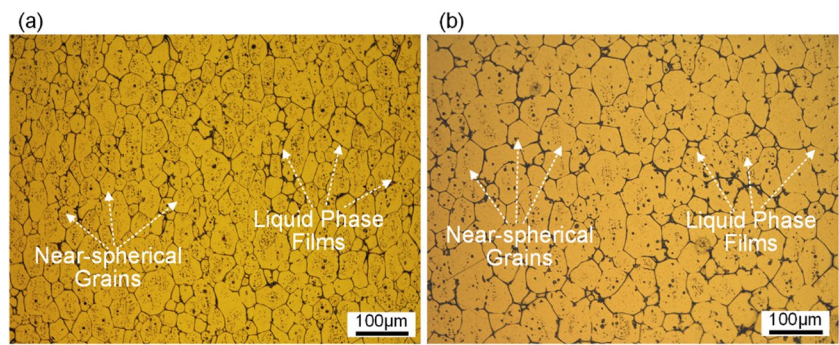


Fig. 9 Microstructure of the 2A50 aluminum alloy semi-solid slurry obtained after holding for 3 min at different temperatures: (a) $575\text{ }^{\circ}\text{C}$ and (b) $590\text{ }^{\circ}\text{C}$



near-spherical grains and intergranular eutectic liquid-phase films were obtained after holding at $575\text{ }^{\circ}\text{C}$ and $590\text{ }^{\circ}\text{C}$ for 3 min, with average grain sizes of approximately $36.5\text{ }\mu\text{m}$ and $42.5\text{ }\mu\text{m}$, respectively.

Inverse pole figure (IPF) maps of the characteristic regions including the tooth, bottom land, and non-dentiform region of the inner gear ring at the extruded temperature of $575\text{ }^{\circ}\text{C}$ and $590\text{ }^{\circ}\text{C}$ are presented in Fig. 10. The white fine solid lines represent the low-angle grain boundaries (LAGBs) at $2^{\circ} < \theta < 15^{\circ}$ (θ represents the misorientation angle), while the black thick solid lines denote the high-angle grain boundaries (HAGBs) ($\theta > 15^{\circ}$). Moreover, the different colors of the grains refer to different crystal orientations. In general, the microstructure of each position of the inner gear ring is composed of fine grains. At the extruded temperature of $575\text{ }^{\circ}\text{C}$, the grains in the tooth were elongated, refined, and clustered along the yellow dashed lines with arrows marked in the tooth, as shown in Fig. 10a. The fine and stretched grains near the edge of the bottom land were arranged along the tooth profile line L1, as shown in region C1 of Fig. 10b. On the contrary, the microstructure of the region at the bottom land but away from the edge was dominated by nearly equiaxed grains, as depicted in region C2 in Fig. 10b. The arrangements of fine and prolonged

grains at the tooth and bottom lands were consistent with the metal flowing during the extrusion, as described in the “Metal flow and strain distribution” section.

When the temperature increased to $590\text{ }^{\circ}\text{C}$, the grains at the tooth and bottom lands became larger, and they were less “elongated” compared to those at $575\text{ }^{\circ}\text{C}$. However, the distribution characteristics of the grains within each region of the inner gear ring remained similar to those at $575\text{ }^{\circ}\text{C}$. The microstructure of the non-dentiform region of the inner gear ring extruded at $575\text{ }^{\circ}\text{C}$ and $590\text{ }^{\circ}\text{C}$ dominated by almost equiaxed grains, the sizes of which were larger than those at the tooth and bottom lands.

Figure 11 demonstrates the grain size (equivalent circle diameter) of the characteristic regions of the inner gear rings shown in Fig. 10. The figures indicate that when the extruded temperature was $575\text{ }^{\circ}\text{C}$, the average grain sizes of the tooth (Fig. 11a) and bottom land (Fig. 11b) were similar, with values of approximately $14.04\text{--}14.62\text{ }\mu\text{m}$. The grain size in the non-dentiform region (Fig. 11c) was $17.04\text{ }\mu\text{m}$. The average grain sizes of the micro inner gear ring increased as the temperature increased to $590\text{ }^{\circ}\text{C}$. Furthermore, the tooth (Fig. 11d) exhibited the highest increment in grain size, approximately 36.3%. At $575\text{ }^{\circ}\text{C}$ and $590\text{ }^{\circ}\text{C}$, the high frequency of grain size statistics appeared in the range of

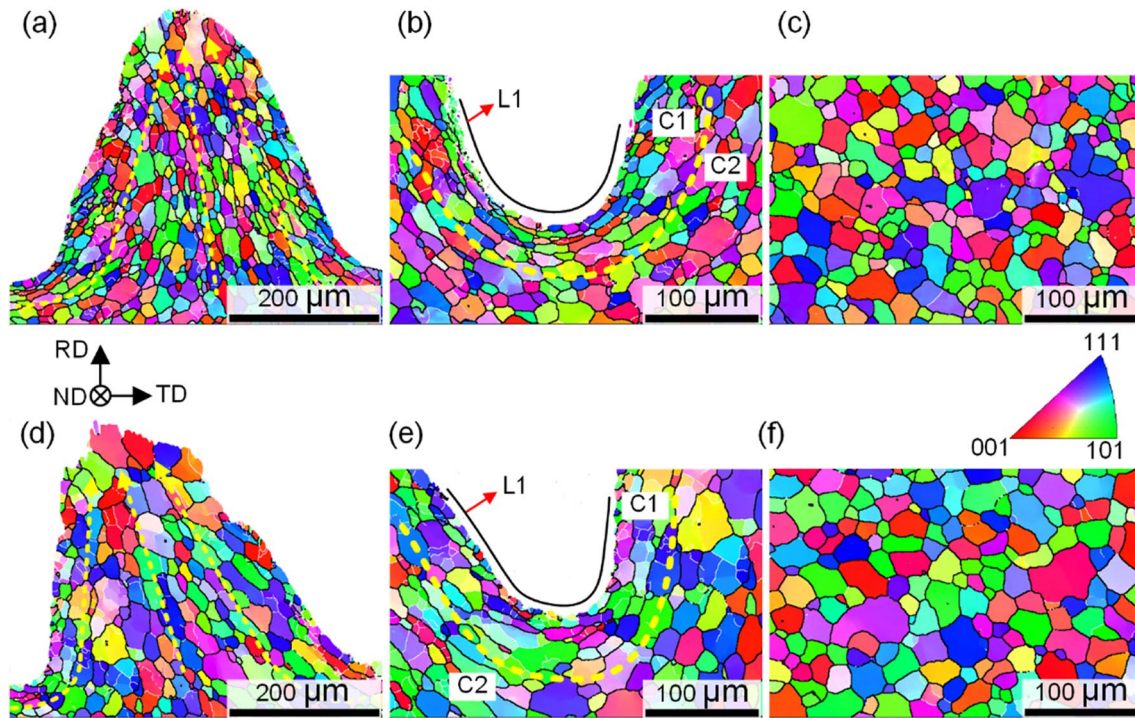


Fig. 10 IPF maps for the characteristic regions of the extruded inner ring gears at different temperatures: (a) tooth, $T=575\text{ }^{\circ}\text{C}$; (b) bottom land, $T=575\text{ }^{\circ}\text{C}$; (c) non-dentiform, $T=575\text{ }^{\circ}\text{C}$; (d) tooth, $T=590\text{ }^{\circ}\text{C}$; (e) bottom land, $T=590\text{ }^{\circ}\text{C}$; and (f) non-dentiform, $T=590\text{ }^{\circ}\text{C}$

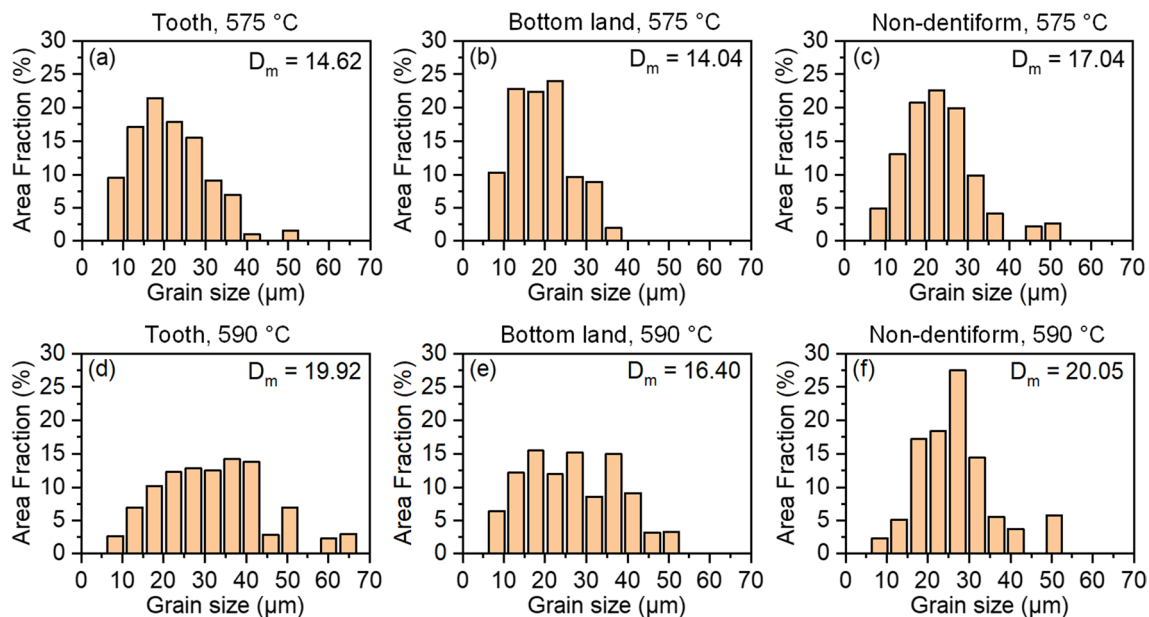


Fig. 11 Grain size distribution of the extruded inner gear rings at different regions: (a) tooth, $T=575\text{ }^{\circ}\text{C}$; (b) bottom land, $T=575\text{ }^{\circ}\text{C}$; (c) non-dentiform, $T=575\text{ }^{\circ}\text{C}$; (d) tooth, $T=590\text{ }^{\circ}\text{C}$; (e) bottom land, $T=590\text{ }^{\circ}\text{C}$; and (f) non-dentiform, $T=590\text{ }^{\circ}\text{C}$

10–30 μm and 15–40 μm , respectively. Furthermore, a small number of grains with size values exceeding 50 μm were more likely to appear at 590 $^{\circ}\text{C}$, indicating that a few grains would evidently grow at elevated extrusion temperature.

Figure 12 illustrates the distribution of grain boundary misorientations of the inner gear rings. The misorientation angles range from 2 to 63 $^{\circ}$ in each region of the inner gear ring, excluding that below 2 $^{\circ}$. Almost all regions

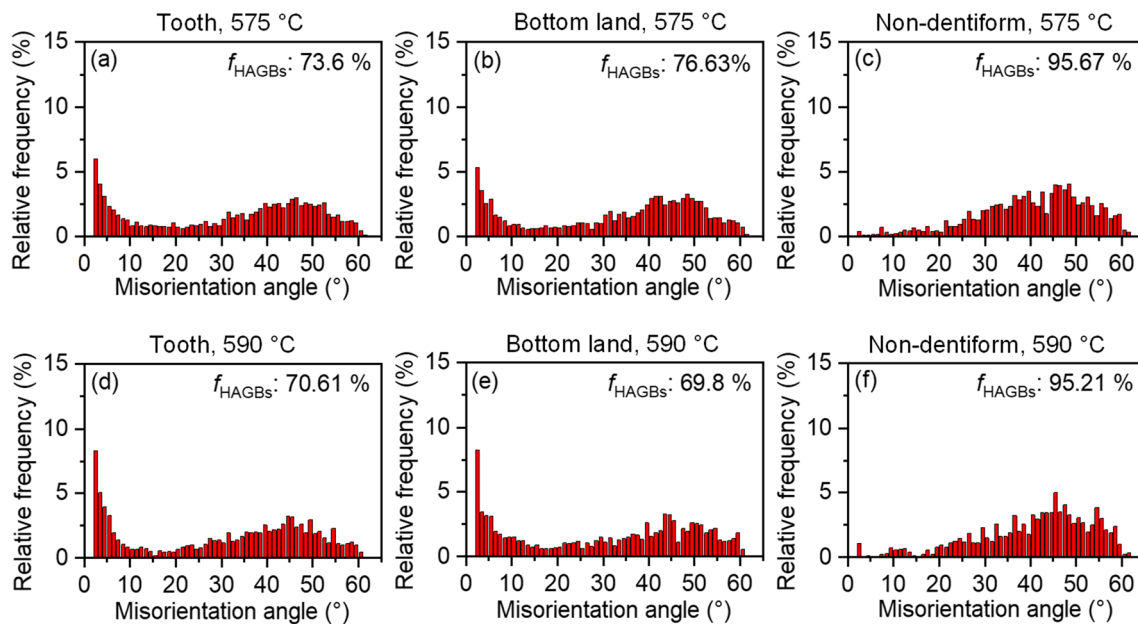


Fig. 12 Misorientation angles distribution of the extruded inner gear rings at different regions: (a) tooth, $T=575$ °C; (b) bottom land, $T=575$ °C; (c) non-dentiform, $T=575$ °C; (d) tooth, $T=590$ °C; (e) bottom land, $T=590$ °C; and (f) non-dentiform, $T=590$ °C

were dominated by HAGBs, among which, the frequency of HAGB at the tooth and bottom lands was 69.8–76.63%. Furthermore, the non-dentiform regions exhibited a HAGBs proportion of more than 90%.

3.3.2 Recrystallization maps

The recrystallization statistics for the internal gear ring are demonstrated in Fig. 13, where the blue color, yellow color, and red color represent the recrystallized grains, substructured grains, and deformed grains, respectively. This figure clearly shows that the microstructure of the inner gear ring predominantly consists of recrystallized and substructured grains. Only a few deformed grains were found at the extrusion temperature of 575 °C. The recrystallization statistics of each region at different extrusion temperatures shown in Fig. 13 were compared. The results show that at the tooth and bottom lands, the recrystallized grains accounted for approximately 40.99–47.28%, and the substructure grains made up about 52.32–58.64%. In contrast, the frequency of recrystallized grains (72.89–80.34%) in the non-dentiform region was significantly higher than the substructure ratio (19.6–27.03%), with almost no deformed grains. At an extrusion temperature of 575 °C, the presence of a few deformed grains suggests that some retained deformation energy. In Fig. 13b, a few red irregular dot-like areas (non-grain shape) are near the edge of the tooth, as highlighted by a green circle, probably caused by the edge-related misinterpretation in the tooth profile.

3.3.3 Texture

Texture has an important influence on the physical and mechanical properties of the alloy, and its effect on material strength depends greatly on the loading direction and the overall orientation of the grains [24, 25]. Pole figure is an important method for characterizing texture. The {100}, {110}, and {111} pole figures of the inner gear rings are illustrated in Fig. 14. The maximum texture intensity of approximately 4.81 was observed in the {100} pole figure for the bottom land at the extruded temperature of 590 °C (Fig. 14e), which was approximately a weak texture of $\{112\} < 126 >$. Besides this maximum, the pole figures of other regions were randomly distributed, with maximum intensity ranging from 2.50 to 4.21, suggesting no evident predominant grain orientations and no strong texture appeared in the majority of the inner gear ring. This finding corresponds to the relatively random distribution of the grain colors, as shown in the IPF maps (Fig. 10).

4 Discussion

4.1 Relationship between metal deformation and microstructure evolution

Figure 10 shows the difference in the shape and size of the grains at each region of the inner gear ring. Figure 6 reveals that the metal flowed intensely and rubbed against the mandrel when it passed through the feature regions, such as

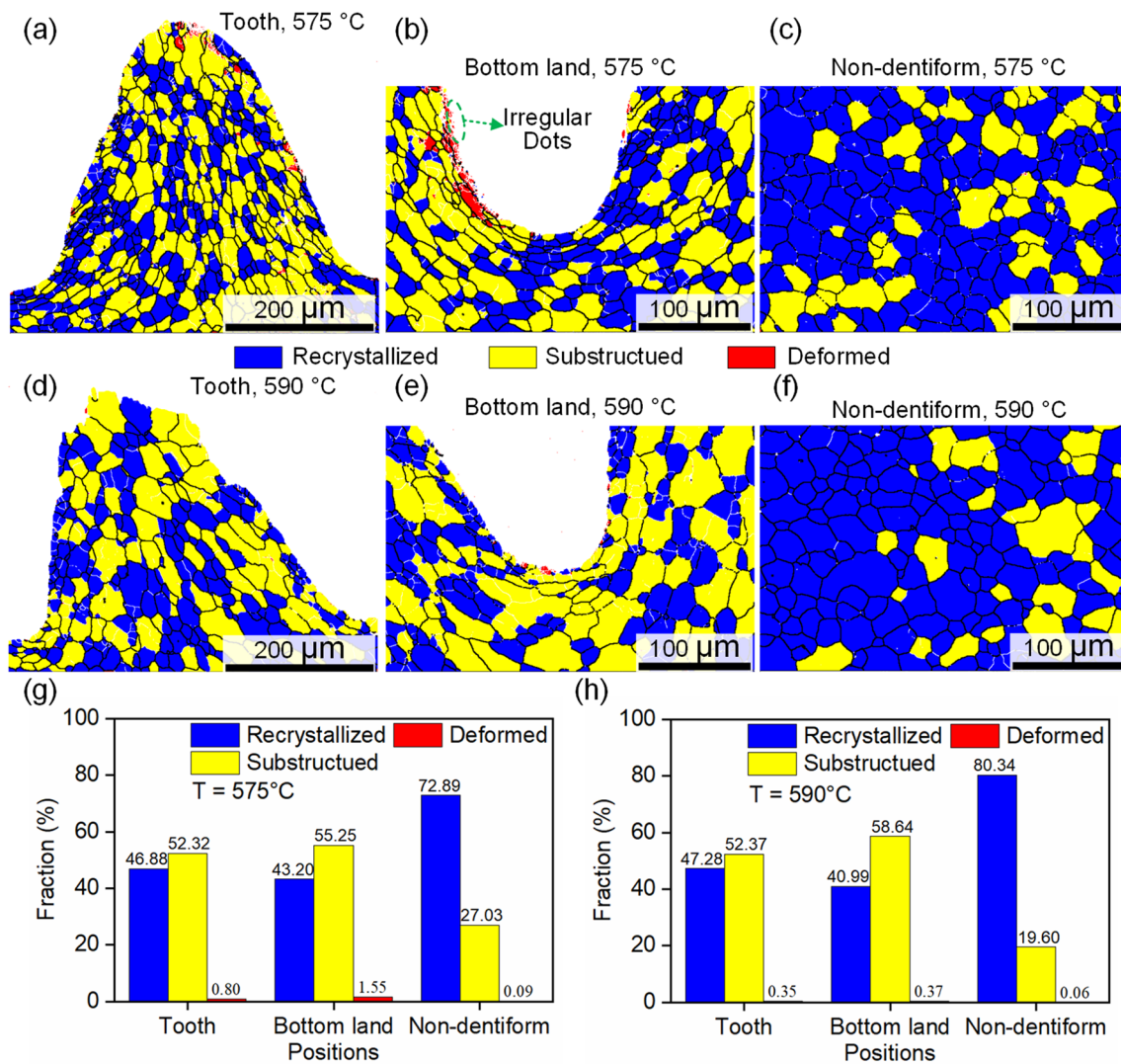


Fig. 13 Microstructure recrystallization diagram of the extruded inner gear rings at different positions: (a) tooth, $T = 575\text{ }^{\circ}\text{C}$; (b) bottom land, $T = 575\text{ }^{\circ}\text{C}$; (c) non-dentiform, $T = 575\text{ }^{\circ}\text{C}$; (d) tooth,

$T = 590\text{ }^{\circ}\text{C}$; (e) bottom land, $T = 590\text{ }^{\circ}\text{C}$; (f) non-dentiform, $T = 590\text{ }^{\circ}\text{C}$; (g) statistics results of the inner gear ring extruded at $T = 575\text{ }^{\circ}\text{C}$; and (h) statistics results of the inner gear ring extruded at $T = 590\text{ }^{\circ}\text{C}$

the top and bottom lands of the mandrel. This interaction results in intense shear deformation of the material, causing larger strain in these regions compared to others, as shown in Fig. 7. While the metal was in the semi-solid temperature, dynamic recovery and dynamic recrystallization could occur substantially in these high-strain regions. Once the extrusion was completed, the dies still maintained a high temperature and promoted the growth of these newly recrystallized grains. In addition, metadynamic recrystallization, static reversion, and static recrystallization may occur at high temperatures when the hot deformation ceases [26–28]. The microstructure of the inner gear ring no longer evolved after removing it from the dies. However, as shown in Fig. 10, the presence of LAGBs in the tooth and bottom lands suggests the potential transformation to HAGBs and possible grain

growth under sustained high temperatures. In the vicinity of the top and bottom lands, a streamlined fibrous microstructure emerges due to the metal flow and the mandrel's constraints during extrusion, evident in the elongated grains of Fig. 10a, b, d, e. Similarly, Zhang et al. [29] observed fine and slender grains parallel to the flank surface at the bottom of the tooth during the rolling process. Moradia et al. [30] noticed that most grains were highly elongated, resulting in a flow pattern in the thermo-mechanically affected zone due to the severe shear and frictional effects of the tool on the material.

However, the metal in the non-dentiform region was primarily compressed toward the center of the billet, with a single arc-shaped die contacting its outer side. The minimal strain was found in the non-dentiform region, as

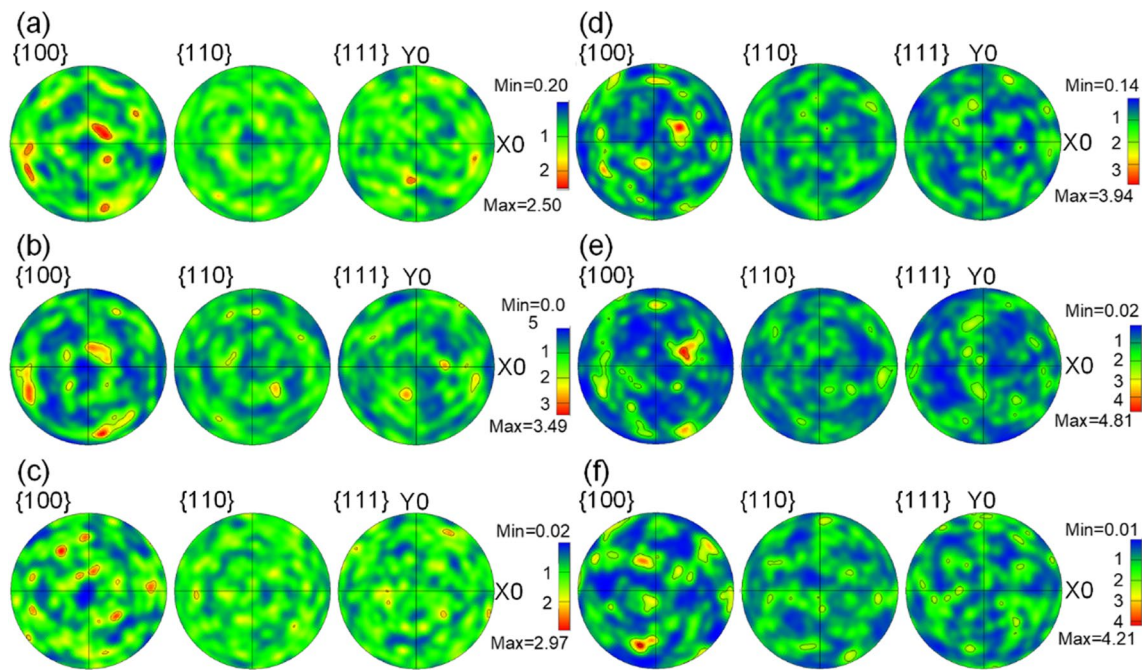


Fig. 14 Pole figures of the characteristic regions of the micro inner gear rings extruded at different temperatures: (a) tooth, $T=575$ °C; (b) bottom land, $T=575$ °C; (c) non-dentiform region, $T=575$ °C;

(d) tooth, $T=590$ °C; (e) bottom land, $T=590$ °C; and (f) non-dentiform region, $T=590$ °C

shown in Fig. 7, where dynamic recrystallization could occur without forming a streamlined fibrous microstructure along the tooth profile. Furthermore, less deformation of the non-dentiform region resulted in a lower dynamic recrystallization level compared to the tooth and bottom lands. Consequently, the microstructure of the non-dentiform region is characterized by nearly equiaxed grains after deformation and recrystallization, not as refined as those in the tooth and bottom lands (Figs. 10, 11, and 13).

The contour lines are distributed relatively randomly in the pole figures (Fig. 14), with a maximum intensity below 5, indicating the absence of strong texture in the inner gear ring [31]. During the rheological extrusion and subsequent cooling process, the microstructure and texture of the inner gear ring were determined by the complex interplay of deformation, recrystallization, and grain growth, as described by Ha et al. [32]. Some preferred orientations may develop as the grains suffered fragmentation, rotation, and translation due to the severe deformation during the extrusion. Recovery and recrystallization occurred in the extrusion and subsequent cooling to consume the stored deformation energy within the grains, leading to the weakening of texture [33]. In addition, further growth of the grains may be unavoidable. After undergoing such complex processes, the newly formed grains no longer exhibit preferred orientations.

4.2 Effect of temperature on the microstructure

In general, aluminum alloy is a material of high stacking fault energy, which undergoes dynamic recovery and dynamic recrystallization during hot deformation processes. As the deformation temperature increases, the dislocations gain more energy to move, resulting in more extensive dynamic recovery and a higher level of dynamic recrystallization [34]. In the rheological extrusion process of the 2A50 aluminum alloy micro inner gear ring, more adequate dynamic recovery and dynamic recrystallization occurred at the extruded temperature of 590 °C compared to 575 °C. During the cooling period of dies, metadynamic recrystallization, static recovery, and static recrystallization could occur simultaneously within the inner gear ring due to the residual high temperature. The grains could grow up in this stage. Moreover, the grain boundaries migrated rapidly as the temperature increased, promoting the grains to grow [35–37]. Consequently, the grains in the microstructure of the inner gear ring at the extruded temperature of 590 °C were larger than that at 575 °C.

The size of the micro inner gear ring is very small, so the average size and number of grains have a great influence on deformation during the rheological extrusion process [38]. The average grain size of the microstructure at 590 °C was larger than that at 575 °C. The number of grains at the tooth decreased with the larger grain size, contributing to poor

coordination of the deformation between neighboring grains in the rheological extrusion process, which had considerable effects on the dimensional accuracy of the micro inner gear ring. Similarly, Meng et al. [39] observed that larger grains led to a few irregular defects on the surface of the flanged micropart fabricated by the hole flanging-ironing process. This demonstrates the impact of the “size effect” on the forming quality of miniature parts manufactured by the plastic forming process. Furthermore, at higher temperatures, the rate of the liquid phase increased, and more liquid phases were squeezed out during the rheological extrusion [40, 41], which may bring about a few defects in the teeth. The combined effect of these factors resulted in a slightly lower dimensional accuracy of the micro inner gear ring at 590 °C compared to 575 °C. This is evident in the more regular macroscopic morphology of the teeth in the micro inner gear ring extruded at 575 °C (Fig. 8), and more homogeneous refined grains were observed (Fig. 10a).

The failure of the micro inner gear rings was usually induced by some defects in weak areas, such as fractures in the top and bottom lands. At 575 °C, the presence of fine and elongated grains in these areas (Fig. 10a,b) can improve the mechanical properties of teeth, potentially increasing the lifespan of the inner gear ring. Nevertheless, at 590 °C, the grains in the bottom land were fine (Fig. 10e), whereas the ones in the tooth were coarse (Fig. 10d), which could negatively affect the overall mechanical performance of the inner gear ring. These findings indicate that a superior microstructure can be obtained when the rheological extrusion is performed at lower semi-solid temperatures, which is beneficial for maintaining the performance of the inner gear ring.

5 Conclusion

In conclusion, the 2A50 aluminum alloy micro inner gear rings were successfully fabricated using the rheological extrusion process in this work, providing a novel approach for manufacturing the components with microfeatures. The metal flow behavior during the extrusion process was analyzed by numerical simulation. Micro inner gear rings were fabricated, and their microstructure was demonstrated in detail by the experiments. The following conclusions can be drawn.

- (1) During the rheological extrusion process, the metal primarily flowed radially along the billet and continuously filled into the tooth spaces of the mandrel. A gradual decrease in metal flow velocity was observed as the extrusion progressed. The values of the metal flow velocity at the tooth and non-dentiform region were reduced from 0.095 to 0.01 mm/s and from 0.084 to 0.06 mm/s, respectively.
- (2) The macroscopic morphology of the extruded micro inner gear rings had no evident defects, and the tooth profile was relatively intact. The elongated grains of the tooth and bottom lands were arranged along the extrusion flowing lines, corresponding to the flow of the material. The grains of the non-dentiform region were nearly equiaxed. The average grain sizes of the teeth and bottom lands (14.04–19.92 μm) were mostly smaller than those in non-dentiform regions (17.04–20.05 μm). The average grain size increased with the elevated extrusion temperature, particularly in the tooth. Some LAGBs were found in the tooth and bottom lands, whereas the non-dentiform region was dominated by HAGBs, with a fraction of 90%.
- (3) The microstructure of the micro inner gear rings of two extruded temperatures was primarily composed of recrystallized and substructured grains, and the frequency of the recrystallized grains in the non-dentiform region was remarkably higher compared to the substructure.
- (4) No strong texture appeared in the microstructure of the micro inner gear ring. Pole figure analyses revealed that the maximum intensity (4.81) occurred in the bottom land of the inner gear ring extruded at 590 °C, indicating an approximately weak $\{112\} <126>$ texture.

Acknowledgements This work was supported by the National Natural Science Foundation of China (Grant No.52105397), the Joint Fund for Aerospace Advanced Manufacturing Technology Research Key Program (Grant No. U1937203), the National Natural Science Foundation of China (Grant No. 52275373), the Research on Innovative Applications of Aerospace Technology (Grant No. 1A0A9FC6), and the Fund of the National Key Laboratory of Metal Forming Technology and Heavy Equipment (Grant No. S2208100.W01).

Data availability The data that has been used is confidential.

Declarations

Competing interests The authors declare no competing interests.

References

1. Nath AG, Sarath Krishnan E, Cheriyan S, Vishnu PS, Krishnan A, Sreedharan P, Udupa G (2018) Design and manufacture of miniature hydraulic gear pump for bio-medical application. *Mater Today: Proc* 5:25570–25580. <https://doi.org/10.1016/j.matpr.2018.10.364>
2. Voyles RM, Godzdzank R (2008) Side-slipping locomotion of a miniature, reconfigurable limb/tread hybrid robot. *IEEE* 58–64. <https://doi.org/10.1109/SSRR.2008.4745878>
3. Chaubey SK, Jain NK (2018) State-of-art review of past research on manufacturing of meso and micro cylindrical gears. *Precis Eng-J Int Soc Precis Eng Nanotechnol* 51:702–728. <https://doi.org/10.1016/j.precisioneng.2017.07.014>

4. Chaubey SK, Jain NK (2019) Analysis and multi-response optimization of gear quality and surface finish of meso-sized helical and bevel gears manufactured by wsem process. *Precis Eng-J Int Soc Precis Eng Nanotechnol* 55:293–309. <https://doi.org/10.1016/j.precisioneng.2018.09.019>
5. Phokane TC, Gupta K, Anghel C (2022) Optimization of gear manufacturing for quality and productivity. *Jurnal Optimasi Sistem Industri* 21:20–27. <https://doi.org/10.25077/josi.v21.n1.p20-27.2022>
6. Li J, Liu H, Shen Z, Qian Q, Zhang H, Wang X (2016) Formability of micro-gears fabrication in laser dynamic flexible punching. *J Mater Process Technol* 234:131–142. <https://doi.org/10.1016/j.jmatprotec.2016.03.018>
7. Yang Y, An Y, Liu X, Jiang Z (2022) A novel process for manufacturing spur gear with uniform microstructure and excellent strength-ductility synergy by warm mold continuous casting. *J Mater Process Technol* 306:117626. <https://doi.org/10.1016/j.jmatprotec.2022.117626>
8. Yan X, Zhang S, Huang K, Yang Y, Wang W, Wu M (2022) Effect of holding time on the extrusion force and microstructure evolution during the plastic forming of Ti-6Al-4V micro-gears. *Materials (Basel)* 15:1507. <https://doi.org/10.3390/ma15041507>
9. Hu C, Lin Q, Shi Y (2021) Micro blanking processing method actuated by piezoelectric ceramic. *Mater Today Commun* 29:102827. <https://doi.org/10.1016/j.mtcomm.2021.102827>
10. Rohmoser A, Kraus M, Leicht M, Merklein M (2022) Experimental evaluation of the feasibility and reproducibility of a novel multi-step forming process for Cu-OFE micro gear manufacturing compared to macro-scale forming. *Manuf Lett* 33:183–189. <https://doi.org/10.1016/j.mfglet.2022.07.024>
11. Jiang C, Chen P, Erisov Y, Chen C (2022) Microforming a miniature cup-shaped internal gear using a cold lateral extrusion process. *Metals (Basel)* 12:826. <https://doi.org/10.3390/met12050826>
12. Yan L, Zhang Z, Li G, Xue Y, Xu J (2021) Evolution of the microstructure, texture and mechanical properties of ZK60 alloy during processing by rotating shear extrusion. *J Alloys Compd* 877:160229. <https://doi.org/10.1016/j.jallcom.2021.160229>
13. Che X, Wang Q, Duan X, Wang M, He L, Cao M, Liu S, Zhang G, Zhang Z (2023) Evolution of microstructure, texture and mechanical properties of AZ80 mg alloy tubular produced by rotating backward extrusion with modified open punch. *J Mater Res Technol* 24:4711–4729. <https://doi.org/10.1016/j.jmrt.2023.04.085>
14. Zhang S, Fan S, Wang Q, Zhao S, Zhu Q (2019) Deformation characteristics of self-infused rolling process for thread shaft. *Int J Adv Manuf Technol* 103:2941–2951. <https://doi.org/10.1007/s00170-019-03677-3>
15. Zeng B, Yan X, Xie Z, Liu J, Wang J, Huang K, Yang Y (2023) Plastic deformation mechanism of the Ti6Al4V micro-gear formed under an electrical field. *Int J Precis Eng Manuf-Green Technol*. <https://doi.org/10.1007/s40684-023-00536-1>
16. Gao X, Wang H, Zhu G, Chang Z, Guo N, Wang Z, Zhu L (2022) Research on metal flow law of micro-riblets based on multi-pass rolling. *J Mech Sci Technol* 36:2277–2286. <https://doi.org/10.1007/s12206-022-0410-5>
17. Liu Y, Xu J, Zhang Z, Liu G, Shan D, Zhang L, Guo B (2022) Micro-extrusion process and microstructure evolution of miniature heat pipe in 6063 aluminum alloy. *Int J Adv Manuf Technol* 120:6463–6480. <https://doi.org/10.1007/s00170-022-09096-1>
18. Wang C, Xue S, Chen G, Cui L, Zhang P (2020) Investigation on formability of bipolar plates during flexible micro forming of Cu/Ni clad foils. *J Manuf Process* 53:293–303. <https://doi.org/10.1016/j.jmapro.2020.02.033>
19. Su Q, Xu J, Yu H, Shi L, Shan D, Guo B (2019) Effect of grain size on formability and deformation mechanism of high-purity aluminum during micro-embossing process at elevated temperature. *Adv Eng Mater* 21. <https://doi.org/10.1002/adem.201900690>
20. Jiang H, An L, Li F, Zhang P, Dong P, Li S, Wang Y, Zhao S (2023) Numerical and experimental study on the rheo-extrusion process of 2A50 aluminium alloy miniature gear. *J Mater Res Technol* 24:1468–1482. <https://doi.org/10.1016/j.jmrt.2023.03.086>
21. Yu J, Zhao G, Chen L (2016) Investigation of interface evolution, microstructure and mechanical properties of solid-state bonding seams in hot extrusion process of aluminum alloy profiles. *J Mater Process Technol* 230:153–166. <https://doi.org/10.1016/j.jmatprotec.2015.11.020>
22. Liu Y, Wang X, Xu J, Shan D, Guo B (2022) Formation mechanism and optimization strategy of surface back-end defects in miniature complex hollow extruded profile. *J Mater Process Technol* 308:117726. <https://doi.org/10.1016/j.jmatprotec.2022.117726>
23. Norton RL (1992) *Design of machinery*. McGraw-hill, New York
24. Shao Z, Lee J, Wang J, Lin J, Jiang J (2020) A study of various heating effects on the microstructure and mechanical properties of AA6082 using EBSD and CPFE. *J Alloys Compd* 818:152921. <https://doi.org/10.1016/j.jallcom.2019.152921>
25. Kocks UF, Tome CN, Wenk HR (1998) *Texture and anisotropy: preferred orientations in polycrystals and their effect on materials properties*. Cambridge University Press, Cambridge
26. Zhang HK, Xiao H, Fang XW, Zhang Q, Logé RE, Huang K (2020) A critical assessment of experimental investigation of dynamic recrystallization of metallic materials. *Mater Des* 193:108873. <https://doi.org/10.1016/j.matdes.2020.108873>
27. Zhao M, Huang L, Zeng R, Su H, Wen D, Li J (2020) In-situ observations and modeling of metadynamic recrystallization in 300m steel. *Mater Charact* 159:109997. <https://doi.org/10.1016/j.matchar.2019.109997>
28. Lin YC, Li L, Xia Y (2011) A new method to predict the metadynamic recrystallization behavior in 2124 aluminum alloy. *Comput Mater Sci* 50:2038–2043. <https://doi.org/10.1016/j.commatsci.2011.02.004>
29. Zhang S, Zhang D, Jiang H, Jiang F, Zhao S (2022) Numerical and experimental analysis of deformation behaviors and microstructure evolution in the thread rolling process. *J Mater Res Technol* 19:230–242. <https://doi.org/10.1016/j.jmrt.2022.05.050>
30. Moradi MM, Jamshidi Aval H, Jamaati R, Amirkhanlou S, Ji S (2019) Effect of sic nanoparticles on the microstructure and texture of friction stir welded AA2024/AA6061. *Mater Charact* 152:169–179. <https://doi.org/10.1016/j.matchar.2019.04.020>
31. Hu Z, Zhang H, Zhu H, Xiao Z, Nie X, Zeng X (2019) Microstructure, mechanical properties and strengthening mechanisms of AlCu5MnCdVA aluminum alloy fabricated by selective laser melting. *Mater. Sci Eng A-Struct Mater Prop Microstruct Process* 759:154–166. <https://doi.org/10.1016/j.msea.2019.04.114>
32. Ha C, Bohlen J, Yi S, Zhou X, Brokmeier H, Schell N, Letzig D, Kainer KU (2019) Influence of Nd or Ca addition on the dislocation activity and texture changes of Mg–Zn alloy sheets under uniaxial tensile loading. *Mater Sci Eng A-Struct Mater Prop Microstruct Process* 761:138053. <https://doi.org/10.1016/j.msea.2019.138053>
33. Zhang D, Liu C, Jiang S, Gao Y, Wan Y, Chen Z (2023) Effects of dynamic recrystallization mechanisms on texture evolution in Mg-Gd-Y-Zr-Ag alloy during hot compression. *J Alloys Compd* 944:169190. <https://doi.org/10.1016/j.jallcom.2023.169190>
34. Li J, Wu X, Liao B, Cao L (2021) Simulation of dynamic recrystallization in an Al-Mg-Si alloy during inhomogeneous hot deformation. *Mater Today Commun* 29:102810. <https://doi.org/10.1016/j.mtcomm.2021.102810>
35. Chamanfar A, Alamoudi MT, Nanninga NE, Misiolek WZ (2019) Analysis of flow stress and microstructure during hot compression of 6099 aluminum alloy (AA6099). *Mater Sci Eng A-Struct Mater Prop Microstruct Process* 743:684–696. <https://doi.org/10.1016/j.msea.2018.11.076>

36. Xu L, Zhou D, Xu C, Zhang H, Qu W, Xie P, Li L (2023) Microstructure evolution, constitutive modeling and forming simulation of AA6063 aluminum alloy in hot deformation. *Mater Today Commun* 34:105138. <https://doi.org/10.1016/j.mtcomm.2022.105138>
37. Zhao J, Deng Y, Tang J, Zhang J (2019) Influence of strain rate on hot deformation behavior and recrystallization behavior under isothermal compression of Al-Zn-Mg-Cu alloy. *J Alloys Compd* 809:151788. <https://doi.org/10.1016/j.jallcom.2019.151788>
38. Marín M, Ortega J, García A, Rubio EM (2023) A review on micro-forming technologies: characteristics and trends for their industrial application. *Procedia Cirp* 118:863–866. <https://doi.org/10.1016/j.procir.2023.06.148>
39. Meng B, Fu MW, Shi SQ (2018) Deformation characteristic and geometrical size effect in continuous manufacturing of cylindrical and variable-thickness flanged microparts. *J Mater Process Technol* 252:546–558. <https://doi.org/10.1016/j.jmatprotec.2017.10.022>
40. Jiang J, Dong J, Huang M, Wang Y, Zhao W (2023) Semi-solid thixotropic behavior and microstructure evolution of cold deformed CoCrCu_{1,2}FeNi high-entropy alloy. *Mater Charact* 201:112926. <https://doi.org/10.1016/j.matchar.2023.112926>
41. Wang Y, Zhao S, Guo Y, Liu K, Zheng S (2021) Deformation characteristics and constitutive equations for the semi-solid isothermal compression of cold radial forged 6063 aluminium alloy. *Materials*. <https://doi.org/10.3390/ma14010194>

Publisher's Note Springer Nature remains neutral with regard to jurisdictional claims in published maps and institutional affiliations.

Springer Nature or its licensor (e.g. a society or other partner) holds exclusive rights to this article under a publishing agreement with the author(s) or other rightsholder(s); author self-archiving of the accepted manuscript version of this article is solely governed by the terms of such publishing agreement and applicable law.